

TARGET SELECTION FOR THE LBTI EXOZODI KEY SCIENCE PROGRAM

ALYCIA J. WEINBERGER

Department of Terrestrial Magnetism, Carnegie Institution for Science, 5241 Broad Branch Road NW, Washington, DC 20015, USA,
weinberger@dtm.cwi.edu

GEOFF BRYDEN

Jet Propulsion Laboratory, California Institute of Technology, 4800 Oak Grove Dr, Pasadena, CA 91109, USA

GRANT M. KENNEDY

Institute of Astronomy, University of Cambridge, Madingley Road, Cambridge CB3 0HA, UK

AKI ROBERGE

Exoplanets & Stellar Astrophysics Laboratory, NASA Goddard Space Flight Center, Code 667, Greenbelt, MD 20771, USA

DENIS DEFRÈRE, PHILIP M. HINZ

Steward Observatory, University of Arizona, 933 N. Cherry Lane, Tucson, AZ, 85721, USA

RAFAEL MILLAN-GABET

NASA Exoplanet Science Institute, California Institute of Technology, Pasadena, CA, 91125, USA

GEORGE RIEKE, VANESSA P. BAILEY

Steward Observatory, University of Arizona, 933 N. Cherry Lane, Tucson, AZ, 85721, USA

WILLIAM C. DANCHI

Exoplanets & Stellar Astrophysics Laboratory, NASA Goddard Space Flight Center, Code 667, Greenbelt, MD 20771, USA

CHRIS HANIFF

Cavendish Laboratory, University of Cambridge, JJ Thomson Avenue, Cambridge CB3 0HE, UK

BERTRAND MENNESSON, EUGENE SERABYN

Jet Propulsion Laboratory, California Institute of Technology, 4800 Oak Grove Dr, Pasadena, CA 91109, USA

ANDREW J. SKEMER

Steward Observatory, University of Arizona, 933 N. Cherry Lane, Tucson, AZ, 85721, USA

KARL R. STAPELFELDT

Exoplanets & Stellar Astrophysics Laboratory, NASA Goddard Space Flight Center, Code 667, Greenbelt, MD 20771, USA

MARK C. WYATT

Institute of Astronomy, University of Cambridge, Madingley Road, Cambridge CB3 0HA, UK

ABSTRACT

The Hunt for Observable Signatures of Terrestrial planetary Systems (HOSTS) on the Large Binocular Telescope Interferometer will survey nearby stars for faint emission arising from ~ 300 K dust (exozodiacal dust), and aims to determine the exozodiacal dust luminosity function. HOSTS results will enable planning for future space telescopes aimed at direct spectroscopy of habitable zone terrestrial planets, as well as greater understanding of the evolution of exozodiacal disks and planetary systems. We lay out here the considerations that lead to the final HOSTS target list. Our target selection strategy maximizes the ability of the survey to constrain the exozodi luminosity function by selecting a combination of stars selected for suitability as targets of future missions and as sensitive exozodi probes. With a survey of approximately 50 stars, we show that HOSTS can enable an understanding of the statistical distribution of warm dust around various types of stars and is robust to the effects of varying levels of survey sensitivity induced by weather conditions.

Subject headings: circumstellar matter

1. INTRODUCTION

The Hunt for Observable Signatures of Terrestrial planetary Systems (HOSTS) on the Large Binocular Telescope Interferometer (LBTI) will survey nearby stars for faint exozodiacal dust (exozodi). This warm circumstellar dust, such as that found in the vicinity of Earth, is generated in asteroidal collisions and cometary breakups. We define exozodiacal dust as sitting in the habitable zone, that is ~ 1 AU from a Solar-type star, and therefore as having a temperature comparable to the Earth, i.e. ~ 278 K.

The goal of the LBTI HOSTS survey is to provide information on exozodi needed to develop a future space telescope aimed at direct detection of habitable zone terrestrial planets (aka. exoEarths). The habitable zone is defined by where a terrestrial planet can have long-term surface water, but its exact boundaries depend on planetary properties. Nevertheless, surface temperatures near 300 K imply that Earth-mass exoplanets need insolation comparable to that of Earth up to 1.2 times greater than Earth’s (e.g. [Leconte et al. 2013](#); [Kopparapu et al. 2013](#)). There is no single agreed upon definition of exozodi in the literature ([Roberge et al. 2012](#)). The HOSTS team has adopted a definition that scales the surface density of the Sun’s Zodiacal disk at the Earth equivalent insolation distance (EEID). Thus the surface density profile expands with stellar luminosity, and allows the “exozodi” level to be compared across stars of different types. See the companion paper [Kennedy et al. \(2014\)](#) for a full discussion of our adopted model. This reference model includes dust interior to the habitable zone all the way in to the sublimation radius, so this model may test how close-in dust such as that detected in near-infrared interferometric surveys ([Absil et al. 2013](#); [Ertel et al. 2014](#)) is related to habitable zone dust.

The typical exozodi detection from space-based photometry and spectrophotometry, primarily with the IRS instrument on the Spitzer Space Telescope, is ~ 1000 times the Solar System’s level (3σ), i.e. 1000 zodi ([Beichman et al. 2006](#); [Lawler et al. 2009](#); [Chen et al. 2014](#)). The best limits from the ground-based Keck interferometer are 500 zodi (3σ) ([Millan-Gabet et al. 2011](#); [Mennesson et al. 2014](#)). Interferometric searches for dust in the near-infrared can find dust interior to the habitable zone, at temperatures $\gtrsim 500$ K ([Absil et al. 2013](#); [Ertel et al. 2014](#)) or that comes from scattered light, and far-infrared and submillimeter telescopes can find dust much cooler than exozodi, at temperatures < 100 K (e.g. [Eiroa et al. 2013](#)). LBTI-HOSTS will be the first survey capable of measuring exozodi known to be at habitable zone temperatures and at the 10-20 zodi level (3σ).

Exozodi of this brightness would be the major source of astrophysical noise for a future space telescope aimed at direct imaging and spectroscopy of habitable zone terrestrial planets. For example, more than about 4 zodis would cause the integration time for coronagraphic imaging of an Earth-like planet in the habitable zone of a G2V star at 10 pc to exceed 1 day, using a 4m telescope and the other baseline astrophysical and mission parameters

given in [Stark et al. \(2014\)](#). A larger telescope can tolerate larger zodi levels for the same integration time.

Detections of warm dust will also reveal new information about planetary system architectures and evolution. Asteroid belts undergoing steady state collisions should grind themselves down in much less time than the Gyr ages of nearby stars. So, warm debris disks around old stars may signal late cometary influxes or stochastic collisional events (e.g. [Wyatt et al. 2007](#); [Gáspár et al. 2013](#)). While $\sim 20\%$ of nearby stars have cold, i.e. < 150 K, dust ([Eiroa et al. 2013](#)) and $\sim 15\%$ have hot, i.e. > 500 K, dust ([Ertel et al. 2014](#)), there is presently no demonstrated connection between the two. To understand the evolution of planetary systems, we seek to measure the luminosity function of exozodi with age and stellar mass and determine whether the presence of cold outer disks correlates with warm inner exozodi.

LBTI is a nulling interferometer, designed to use the 8.4 m apertures of the LBT fixed in a common mount at a 14.4 m separation, for the detection of emission from warm dust around nearby stars. LBTI works in the thermal infrared, employing dual adaptive secondaries to correct atmospheric seeing, and providing low thermal background and high Strehl images to the science camera NOMIC ([Hinz et al. 2008, 2012](#)). Closed loop phase tracking in the near infrared is used to stabilize the destructive interference of the star at N-band (9.8-12.4 μ m) and detect flux from the resolved dust disk [Defrère et al. \(2014\)](#). The separation of the LBT mirrors at a working wavelength of 11 μ m produces a first transmission peak centered at 79 mas (1 AU at 13 pc) and an inner working angle (half transmission) of 39 mas (1 AU at 25 pc).

Together, observations of thermal emission from disks with LBTI and images with space-based optical coronagraphs capable of probing the same angular scales in scattered light will measure the albedo of dust grains. Albedo is one of the few available constraints on dust composition and thereby parent body composition for debris disks. Scattered light images of dust in the habitable zones of several nearby stars may be possible with a coronagraph on the WFIRST-AFTA mission ([Spergel et al. 2013](#)).

2. TARGET LIST ASSEMBLY AND EXCLUSIONS

2.1. Target Selection Goals

Target selection for HOSTS is a balance between including stars that are expected targets of a future exoEarth mission and including stars of various types to enable the best understanding of the statistical distribution of exozodi over a range of parameters. The two approaches are complementary and together enable investigations of habitable zone dust production across a range of host stellar types.

The mission-driven approach concentrates on F, G, and K-type stars that are the best targets for future direct observations of exoEarths, thereby providing “ground truth” dust observations. The sensitivity sweet spot for an optical planet imager lies with G and K stars because 1) the planet-to-star contrast ratio is inversely proportional to stellar luminosity and 2) the orbital ra-

dius of the habitable zone increases as $\sqrt{L_*}$ ¹. As a result, M-type stars have favorable planet-to-star contrast ratios but habitable zones close to the stars, whereas A-type stars have poor contrast ratios and habitable zones further from the stars.

Not every potential target of a future exoEarth mission can be observed with LBTI; for one thing, many lie in the southern hemisphere and are not observable from LBT on Mount Graham, AZ. Furthermore, some stars bright enough at visual wavelengths and therefore accessible to an exoEarth mission would be too faint for LBTI to achieve good sensitivity in the limited total observing time. Our goal is to design a survey that can fully inform target selection for a future exoEarth mission; survey results will have to be modeled and then extrapolated to lower dust levels. Therefore, there must be observational extensions to the mission-driven sample that will inform models of dust evolution and aid extrapolation.

The second approach, a LBTI sensitivity-driven approach, selects targets based only on the expected LBTI exozodi sensitivities, without consideration of exoEarth mission constraints. This would naturally select more early-type stars (A stars and early F-type stars) because they are brighter, have habitable zones at large separations, and higher F_{disk}/F_* at N-band (see Kennedy et al. (2014) for details). Therefore, the results of this type of survey would have to be extrapolated to later spectral type targets using planet formation theory.

The brightest nearby late-F to K-type stars can satisfy both the mission and sensitivity-driven selection criteria, and we give a description of these in Section 3, we show that there are 25-48 such stars, depending on LBTI sensitivity. We anticipate that HOSTS will survey ~ 50 stars, given the amount of observing time allocated on LBTI, so the target selection approach followed will determine the rest of the observed stars.

We lay out here the considerations that lead to the final HOSTS target list. We discuss how to balance mission-driven and sensitivity considerations to maximize scientific return from the HOSTS project. By presenting our target list in this early paper, we also hope to encourage intensive study of these stars with other techniques that will eventually enhance our ability to understand the evolution of circumstellar dust with time.

2.2. Target Selection Constraints

We started with a list of all bright, northern main sequence stars of spectral types A through M observable from LBT (declination $> -30^\circ$) by using two catalogs: the Unbiased Nearby Stars (UNS) sample assembled for cold debris disks studies (Phillips et al. 2010) and the Hipparcos 30 pc sample assembled for exoEarth mission planning (Turnbull et al. 2012). UNS is complete

¹ The EEID, i.e. where a planet receives the same incident flux as Earth, defines the habitable zone (see Section 3). Since the flux at the EEID is a constant, a $1 R_\oplus$ planet there always has the same absolute magnitude independent of host star luminosity. However, the absolute magnitude of stars decreases toward earlier spectral type stars, thus increasing the star-to-planet flux ratio. The radial temperature dependence of a blackbody emitter in a stellar radiation field can be calculated by equating the incident flux ($L_*/4\pi r^2$) with the emergent flux ($4\sigma_{\text{EEID}}^2 T_{\text{HZ}}^4$). Thus, for a fixed temperature, as in a habitable zone, the radius at which a blackbody reaches that temperature is proportional to \sqrt{L} .

to about 16 pc for K-type stars and about 45 pc for A-type.

Binary stars were excluded based on both technical and scientific criteria. There are two technical reasons to exclude binary stars: 1) to ensure that the adaptive optics system can easily lock on the target of interest and 2) to ensure that flux from the companion does not contaminate the area being searched for exozodi emission. We therefore excluded binary stars with separations $< 1''5$. Some stars are known to be spectroscopic binaries (SBs) but without well-measured orbits. We excluded all such SBs because their maximum separations might fall within an angular range of 10s to 100s of mas and provide confusing non-null signals. The main sources of information about multiplicity were the Washington Visual Double Star Catalog (Mason et al. 2013) and the 9th Catalogue of Spectroscopic Binary Orbits (Pourbaix et al. 2009).

We further excluded stars with flux densities < 1 Jy in the broad N-band ($\sim 11 \mu\text{m}$) filter used for the HOSTS survey. We anticipate that the LBTI null would be degraded for fainter stars. To estimate the brightness of our targets, we fit Kurucz stellar models to available photometry at BVJHK plus WISE bands W3 ($12 \mu\text{m}$) and W4 ($22 \mu\text{m}$) and then used the model to predict the NOMIC flux density.

We also only considered stars with inner habitable zone distances probed by the LBTI transmission pattern, i.e. zones larger than about 60 mas. An exozodi disk smaller than this has low transmission efficiency, i.e. it is nulled along with the star because the LBTI transmission pattern peak is at ≈ 79 mas. A general result of our brightness cuts is that our target stars are all within 28 pc. Therefore, our angular criterion, above, excluded binaries with separations $\lesssim 50$ AU. Furthermore, studies of protoplanetary disk evolution indicate that stellar companions within 100 AU of the primary stars cause lower disk masses and faster disk dissipation, possibly inhibiting planet formation (e.g. Osterloh & Beckwith 1995; Jensen et al. 1996; Andrews & Williams 2005; Harris et al. 2012). We therefore also excluded physical binaries with separations < 100 AU. Although it would be interesting to study the effect of binary separation on habitable zone dust, we emphasized the formation of an overall sample with as few selection effects as possible and eschewed inclusion of subsamples too small to provide statistically meaningful results.

Finally, we excluded giant stars (luminosity class III), i.e. stars that appear significantly brighter than the main sequence. LBTI would probe regions around these stars that are significantly larger than the size of the habitable zones that existed when the stars resided on the main sequence and thus not directly comparable to the rest of the sample. Table 3 lists the targets excluded for binarity and location above the main sequence.

2.3. Target List Categories

We categorize the targets that meet the above criteria into two samples described below in:

Section 3: The Sun-like sample includes targets with spectral types later than F5. These 48 stars are potential targets for a future exoEarth mission. Of these 25 have flux density > 2 Jy at N-band.

Section 4: The sensitivity-driven, i.e. early-type star, sample includes targets with spectral types between A0 and F4. These 20 stars provide additional information on the exozodi luminosity function. Of these, 15 have flux density $>2\text{Jy}$ at N-band.

Together, there are 68 sources in the above categories from which the optimal HOSTS survey can be created.

3. SUN-LIKE SAMPLE

Our objective for this LBTI-HOSTS sub-sample is to observe stars that are probable targets for a future exoEarth mission, based on current knowledge, and stars that inform our understanding of the typical exozodi levels around similar stars. These observations will provide dust measurements (or upper limits) for specific stars. They will also supply a larger sample of solar-type stars with which to model the distribution of exozodi levels for Sun-like stars. This will enable evaluation of the suitability, as exoEarth mission targets, of individual stars that could not be observed from LBTI (because, for example, they were too faint or too far south). Here, we define “Sun-like” as having spectral types later than or equal to F5. The coolest star that passed all our cuts is spectral type K8. The majority of high photometric quality targets for the Kepler mission’s exoplanet search are also of spectral types mid-K to mid-F (4500-7000 K) (Christiansen et al. 2012).

The great technical challenge for direct exoEarth observations is to suppress the central starlight tremendously yet allow light from extremely faint planets to be detected at small angular separations. Therefore, the best systems to search for exoEarths are those with widely separated habitable zones (HZs) and with high planet-to-star flux ratios. A full discussion of all the considerations that go into determining a star’s habitable zone boundaries appears in Kopparapu et al. (2013). However, to first order, the location of a star’s HZ is set by how much light would hit an Earth-twin planet. Therefore, the Earth-equivalent insolation distance (EEID) approximately scales in the following way

$$r_{\text{EEID}} \approx r_{\oplus} \times (L_{\star} / L_{\odot})^{1/2}, \quad (1)$$

where L is the bolometric luminosity and r_{\oplus} is the Earth-Sun distance.

Following Turnbull et al. (2012), the planet-to-star reflected flux ratio at visible wavelengths for an Earth-twin planet is approximately

$$(F_p / F_{\star})_{\text{HZ}} \approx (1.2 \times 10^{-10}) / (L_{\star} / L_{\odot}) \quad (2)$$

So as the stellar luminosity increases, the HZ moves outwards, increasing the separation of an exoEarth from its host star (good). However, simultaneously the planet-to-star flux ratio decreases, resulting in longer exposure times to reach a given detection limit (bad).

These two competing effects largely dictate which stars are the best for direct observations of exoEarths. The current consensus is that starlight suppression technologies working at optical wavelengths (e.g. internal coronagraphs) are the most advanced (Greene et al. 2013). For these mission concepts, the best targets are nearby stars of mid-F, G, and K spectral types. In general, for a given optical coronagraphic telescope aperture, the less exozodi noise contribution that a star system has, the earlier the

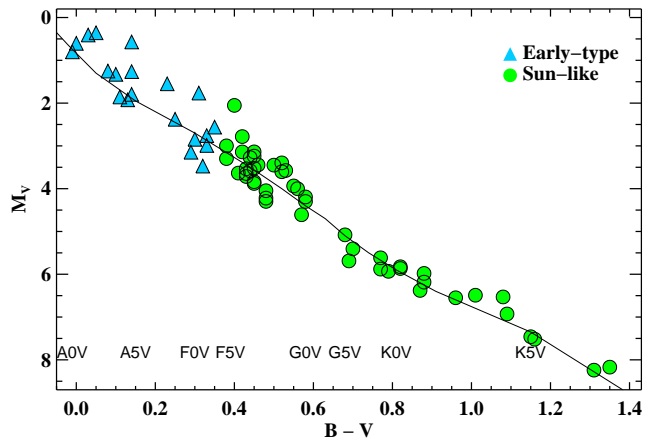


Figure 1. Color magnitude (absolute V magnitude versus B-V color) plot of the complete sample. Sun-like stars, defined as spectral type F5 and later, are shown with green filled circles. Early type stars, defined as spectral types F4 and earlier, are shown with blue filled triangles. The black line shows the MK main sequence as given in Drilling & Landolt (2000).

spectral type of star systems that can be searched with high completeness. An interferometric mission, such as an array of $4 \times 4\text{m}$ free-flying mid-infrared telescopes, provides somewhat different completeness as a function of stellar luminosity. For the HOSTS survey, we make no assumptions about exoEarth detection technology. If we keep the ratio of F:G:K stars fixed, the best targets for an interferometric telescope agree well with the coronagraphic telescope list (Defère et al. 2010).

We found 48 stars that met all of our selection criteria and some of their basic properties are listed in Table 1 and shown in Figures 1 and 2. Our current working knowledge of the LBTI system is that the null quality will not depend on stellar brightness for stars brighter than 2Jy at N-band; there are 25 such bright stars on our list. We expect that for stars fainter than 2Jy , the degradation in the null will be a gentle function of brightness, but this remains to be tested.

The mean distance to these sample stars is 11.4pc ; the closest star is at 3.2pc and the most distant at 21.4pc . The presence/absence of a disk was not a criterion for selecting stars in the Sun-like star sample. What is known about the presence or absence of hot/warm (potentially N-band detectable) and cold (far-IR detectable) circumstellar disks is noted in the Table. Each dust survey has somewhat different limits; the reader should consult the original papers for details.

4. SENSITIVITY-DRIVEN, I.E. EARLY-TYPE, SAMPLE

Our objective for this sample is to find stars for which LBTI can make its most sensitive observations of $\sim 300\text{K}$ dust, regardless of the spectral type of the host star. To create this sample, we select all stars that have N-band flux densities $\geq 1\text{Jy}$ and for which the location of the EEID is $>60\text{mas}$. This preferentially selects A-type and early F-type stars. In general, these are not good exoEarth imaging targets themselves, because of the low habitable-zone-planet-to-star contrast. However, they will provide an important addition to our understanding of the exozodiacal dust luminosity function as it might depend on mass and luminosity of the host star.

We find an additional 20 stars that meet our selection criteria and were not already selected in the Sun-like

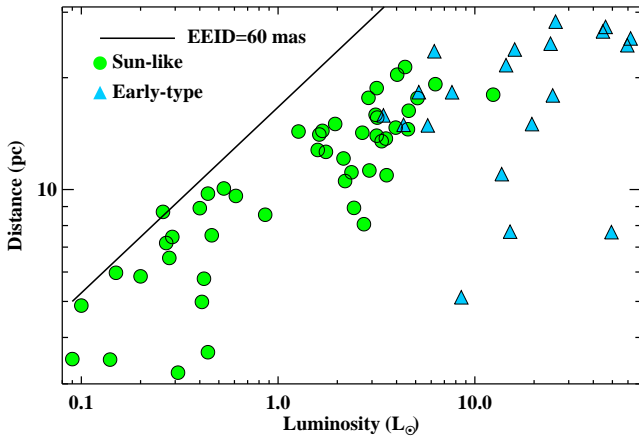


Figure 2. Distance versus luminosity for the complete sample. The black line shows an Earth equivalent insolation distance (EEID) of 60 mas. Stars that fall above this line were excluded because their exozodi would largely fit within the first null, and therefore LBTI would not be very sensitive to such dust. The LBTI the inner working angle in N-band ($11 \mu\text{m}$), defined as $\lambda/4B$, is ≈ 39 mas for the LBT mirror separation of 14.4 m while the first transmission peak is at 79 mas. That stars $>1 L_{\odot}$ fall well below the line shows that the N-band flux density requirement drives the source selection rather than the EEID requirement.

Sample. These stars are all earlier spectral type than F4 and are given in Table 2. These stars are typically further away than the Sun-like sample stars, with an average distance of 18.6 pc. Twelve stars have significant infrared excesses indicating abundant circumstellar dust at some distance from the stars; references are given in the table.

5. DISCUSSION

Despite our attempts to reject known binaries (see Section 2.2), there could be unknown companions that would transmit through the LBTI null pattern and therefore generate some signal. There are some ways to distinguish a companion from a disk using LBTI. A companion will transmit primarily through a single LBTI fringe, unlike a spatially resolved disk. Therefore, a companion will produce a null that varies as the orientation of the projected baseline of the interferometer changes due to Earth’s rotation over an observation. However, an inclined disk would have a similar effect; therefore distinguishing a companion from a disk will likely require follow-up observations. For example, measuring the source null in narrower filters at the short and long wavelength ends of N-band, i.e. 8 and $12.5 \mu\text{m}$, would provide some information on its temperature and spatial extent. Radial velocity observations will constrain the possible masses and orbital periods of suspected companions.

Any companions discovered by LBTI are likely to be of substellar mass. All but four of the Sun-like sample stars and seven of the Early-type sample stars have been studied extensively by radial velocity planet search programs (e.g. Butler et al. 2006; Lagrange et al. 2009; Fischer et al. 2014). At the separation of maximum transmission, i.e. 79 mas, a $80 M_{\text{Jup}}$ brown dwarf in an orbit inclined at 45° would induce a typical reflex motion of about 2 km s^{-1} for our sample stars, which could be detected for all but the most rapidly rotating stars in the sample.

In advance of scheduled HOSTS observing runs, a pri-

oritized list of targets will be constructed based on the target observability (e.g. above airmass 1.5 for more than 2 hr) and our expected sensitivity to exozodi. To determine our expected sensitivity, we pass an exozodi model, described in Kennedy et al. (2014), through an LBTI null model to calculate an exozodi limit for each star, in the unit of a “zodi.” This model was designed to be simple, to facilitate comparisons between observations of stars of varying properties, and to have a straightforward correspondence with the Solar System’s actual Zodiacal cloud. The basic features of this model are a fixed surface density in the habitable zone, i.e. at a temperature of 278 K, and a weak power law dependence of surface density on radius from the star that matches the Zodiacal cloud’s. Figure 3 shows this estimation based on current knowledge of the achievable LBTI null depth. LBTI is still in commissioning, so the final dependence of null depth on target brightness is not yet well established. We have assumed that for targets brighter than 2 Jy, LBTI will be systematics limited, so the target’s flux density will not affect our zodi sensitivity. However, there may be additional degradation of the null for targets of 1–2 Jy, which comprise 28/68 of our targets.

There are many other possible definitions of a “zodi” including ones defined in terms of a fixed $F_{\text{dust}}/F_{\star}$ or $L_{\text{dust}}/L_{\star}$ at a given temperature (Roberge et al. 2012). For comparison purposes, we also calculate an exozodi sensitivity for each of our target stars by assuming a version of our reference model that contains dust only in the habitable zone, i.e. extending from 0.95 - $1.37 \sqrt{L_{\star}}$ and normalized to a fixed $F_{\text{dust}}/F_{\star} = 5 \times 10^{-5}$ at a wavelength of $11 \mu\text{m}$ (for our NOMIC filter). These limits are also shown in Figure 3.

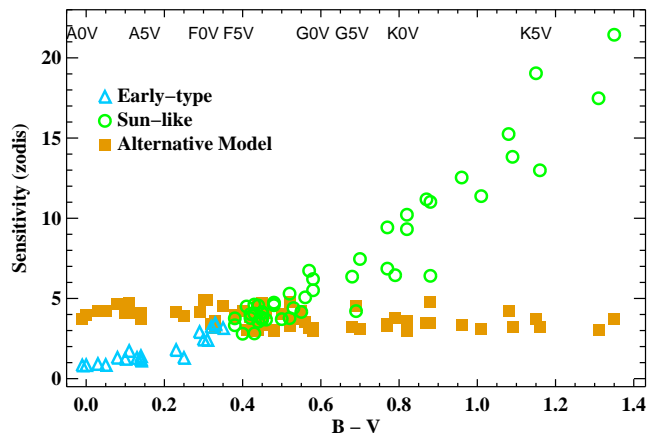


Figure 3. Expected LBTI sensitivity (1σ) to dust, in zodis as defined in Kennedy et al. (2014) and assuming a null depth of 10^{-4} for the complete sample (green and blue circles). In this model, the surface density of the disk in the habitable zone is fixed and the flux density of the disk relative to the star is $\propto T_{\star}^3$, so LBTI is more sensitive to dust around hotter (bluer) stars. Note that these values of the sensitivity assume that the null is limited by systematics and not by target flux density. An alternative definition of a zodi is a fixed flux density in the habitable zone (orange squares); in this case LBTI’s limits are only weakly a function of stellar luminosity.

The goal of the overall survey is not only to identify exozodiacal dust around specific stars of interest, but also to measure the luminosity function of disks in a general statistical sense. As such, we define here a key metric

for the overall survey - Z_{10} - the fraction of stars with more than 10 zodis. This level of exozodi, versus a Solar System level of dust, would cut the number of Earth-like planets imaged by a future direct-imaging mission by half (Stark et al. 2014). This recent work also shows, however, that a mission that observes an ensemble of stars has a total planet yield that is a weak function of the exozodi level (Stark et al. 2014).

In a real-world ground-based observing program, under changing seeing and transparency and seasonally biased conditions, it will be impossible to observe all stars, even those brighter than 2 Jy, to identical zodi detection depths. Of the 68 stars in Tables 1 and 2, we expect to observe ~ 50 . What is critical is that no biases to the sample are introduced during the selection of the actual observed targets.

The ability of the LBTI survey to constrain Z_{10} depends on both the number of observed targets and the sensitivity of each individual measurement. We performed Monte Carlo simulations to estimate the expected accuracy of Z_{10} as a function of the number of targets. Assuming that the underlying distribution of disk brightnesses follows a log-normal distribution whose width is set by Z_{10} , we determine how well Z_{10} is constrained by the LBTI observations. We assume that each star is treated as a unique observation. The bright end of the distribution is already constrained by Spitzer/KIN/WISE observations (Lawler et al. 2009; Millan-Gabet et al. 2011; Kennedy & Wyatt 2013); therefore, we set the frequency of 1000 zodi disks to be 1%.

At first we consider a uniform survey depth with 3-zodi sensitivity for each measurement ($1-\sigma$), which we assume would be the perfect, likely unachievable, survey LBTI could perform. Figure 4 shows how well Z_{10} is constrained by uniform-depth surveys ranging from 30 to 70 stars. We find that a 50 star survey can measure Z_{10} with $\sim 20\%$ accuracy (for $Z_{10} \approx 0.3-0.4$). Using advanced statistical methods to allow averaging over multiple targets to achieve deeper zodi limits, it may be possible to improve on these rough limits (Mennesson et al. 2014).

Since variations in weather will inevitably result in non-uniform sensitivity, Figure 4 also shows the constraints on Z_{10} for a 2-layered survey, where 40 stars are observed with 3-zodi accuracy and another 30 stars with only 10-zodi accuracy. We find that this layered survey has equivalent power to reveal the zodi luminosity function as a 50 star survey done to a depth of 3 zodis. We conclude that an optimal observing strategy should not mandate uniform sensitivity, thereby concentrating a large fraction of telescope time on a small number of stars, but will instead observe a greater number of stars, some with greater depth than others.

The HOSTS survey is expected to begin in 2015 and to continue for two to three years. During commissioning, LBTI observed η Crv, one of the early-type sample stars with a known mid-infrared excess. The observations demonstrate the power of LBTI to constrain the dust distribution in the habitable zone (Defrere et al. 2014).

The Large Binocular Telescope Interferometer is funded by the National Aeronautics and Space Admin-

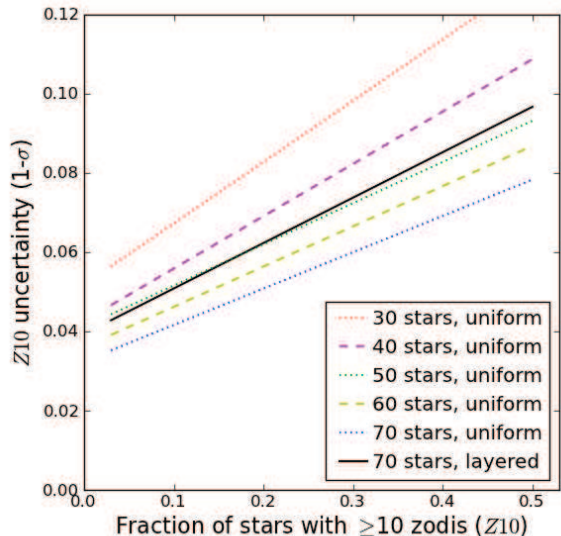


Figure 4. The ability of the overall survey to constrain Z_{10} (the fraction of stars with ≥ 10 zodis of dust) depends on the number of targets and the accuracy of each measurement. Based on Monte Carlo simulations we find that a survey with two levels of sensitivity - 40 stars with 3-zodi accuracy and 30 stars with 10-zodi accuracy (black line) - is roughly equivalent to a 50 star survey of uniform 3-zodi depth (green dashed line).

istration as part of its Exoplanet Exploration Program. This work of GMK & MCW was supported by the European Union through ERC grant number 279973. This research has made use of the SIMBAD database and the VizieR catalogue access tool, CDS, Strasbourg, France and the Washington Double Star Catalog maintained at the U. S. Naval Observatory.

6. APPENDIX: BINARY STARS EXCLUDED FROM SAMPLE

We list here (Table 3) stars that could otherwise meet our selection criteria but that were excluded due to binarity as described in Section 2.2. Much of the information in this table comes from Washington Double Star Catalog (Mason et al. 2001-2014).

REFERENCES

- Absil, O., Defrère, D., du Foresto, V. C., et al. 2013, *A&A*, A104
 Andrews, S. M., & Williams, J. P. 2005, *The Astrophysical Journal*, 631, 1134
 Beichman, C. A., Bryden, G., Stapelfeldt, K. R., et al. 2006, *ApJ*, 652, 1674
 Bryden, G., Beichman, C. A., Trilling, D. E., et al. 2006, *ApJ*, 636, 1098
 Bryden, G., Beichman, C. A., Carpenter, J. M., et al. 2009, *ApJ*, 705, 1226
 Butler, R. P., Wright, J. T., Marcy, G. W., et al. 2006, *ApJ*, 646, 505
 Chen, C. H., Mittal, T., Kuchner, M., et al. 2014, *ApJS*, 211, 25
 Chen, C. H., Patten, B. M., Werner, M. W., et al. 2005, *ApJ*, 634, 1372
 Christiansen, J. L., Jenkins, J. M., Caldwell, D. A., et al. 2012, *PASP*, 124, pp. 1279
 Defrère, D., Absil, O., den Hartog, R., Hanot, C., & Stark, C. 2010, *A&A*, 509, A9
 Defrere, D., Hinz, P. M., Sekmer, A. J., et al. 2014, *ApJ*, in press
 Defrère, D., Hinz, P., Downey, E., et al. 2014, in *SPIE Conference Series*, Vol. 9146, 914609-914609-8
 Drilling, J. S., & Landolt, A. U. 2000, in *Allen's Astrophysical Quantities*, ed. A. N. Cox (New York: AIP Press), 381

Table 1
Stars in the Sun-like Star Sample

HD	Name	RA	Dec	Distance (pc)	Spectral Type	EEID	F_{ν} (N-band) (Jy)	hot/warm excess	cold excess
693	6 Cet	00:11:15.86	-15:28:04.7	18.7	F8V	0.095	1.15		n (E13)
4628		00:48:22.98	+05:16:50.2	7.5	K2.5V	0.072	1.30		n (T08)
9826	ν And	01:36:47.84	+41:24:19.6	3.5	F9V	0.136	2.36	n (A13)	n (B06,E13)
10476	107 Psc	01:42:29.76	+20:16:06.6	7.5	K1V	0.090	2.02	n (MG11)	n (T08)
10700	tau Cet	01:44:04.08	-15:56:14.9	3.6	G8.5V	0.182	5.42	y (A13)	y (G04)
10780	GJ 75	01:47:44.83	+63:51:09.0	10.1	K0V	0.072	1.12		n (L09)
16160	GJ 105	02:36:04.89	+06:53:12.7	7.2	K3V	0.073	1.53		n (T08)
16895	13 Per	02:44:11.99	+49:13:42.4	11.1	F7V	0.138	2.43	n (A13)	n (Be06)
17206	tau01 Eri	02:45:06.19	-18:34:21.2	14.2	F75	0.115	1.69		n (T08)
19373	iot Per	03:09:04.02	+49:36:47.8	10.5	F9.5V	0.141	2.85	n (MG11)	n (T08)
22049	eps Eri	03:32:55.84	-09:27:29.7	3.2	K2V	0.172	7.39	n (A13)	y (B09)
22484	LHS 1569	03:36:52.38	+00:24:06.0	14.0	F8V	0.127	2.35	y (A13)	y (T08)
23754	tau06 Eri	03:46:50.89	-23:14:59.0	17.6	F5IV-V	0.128	2.10		n (G13)
26965	omi Eri	04:15:16.32	-07:39:10.3	5.0	K0.5V	0.128	3.51		n (L02)
30652	1 Ori	04:49:50.41	+06:57:40.6	8.1	F6V	0.205	4.76	n (A13)	n (T08)
32147		05:00:49.00	-05:45:13.2	8.7	K3V	0.059	1.00		n (L09)
34411	lam Aur	05:19:08.47	+40:05:56.6	12.6	G1.5IV	0.105	1.80	n (MG11)	n (T08)
35296	V1119 Tau	05:24:25.46	+17:23:00.7	14.4	F8V	0.090	1.03		n (T08)
38393	gam Lep	05:44:27.79	-22:26:54.2	8.9	F6V	0.175	4.40	n (MG11)	n (Be06)
48737	ksi Gem	06:45:17.36	12:53:44.13	18.0	F5IV	0.196	4.34	n (A13)	n (K13)
78154	sig02 Uma A	09:10:23.54	+67:08:02.4	20.4	F6IV	0.099	1.24		n (G13)
84117	GJ 364	09:42:14.42	-23:54:56.0	15.0	F8V	0.093	1.11		n (E13)
88230	NSV 4765	10:11:22.14	+49:27:15.3	4.9	K8V	0.065	1.91	n (MG11)	n (T08)
89449	40 Leo	10:19:44.17	+19:28:15.3	21.4	F6IV	0.098	1.10		n (G13)
90839	36 Uma	10:30:37.58	+55:58:49.9	12.8	F8V	0.099	1.25		n (T08)
95128	47 Uma	10:59:27.97	+40:25:48.9	14.1	G1V	0.091	1.35	n (MG11)	n (T08)
101501	61 Uma	11:41:03.02	+34:12:05.9	9.6	G8V	0.081	1.24		n (G03)
102870	bet Vir	11:50:41.72	+01:45:53.0	10.9	F9V	0.173	4.30	n (A13)	n (T08)
115617	61 Vir	13:18:24.31	-18:18:40.3	8.6	G7V	0.108	2.20	n (L09,E14)	y (L09)
120136	tau Boo	13:47:15.74	+17:27:24.8	15.6	F6IV	0.114	1.67	n (E14)	n (B09)
126660	tet Boo	14:25:11.8	+51:51:02.7	14.5	F7V	0.147	3.12		n (T08)
131977	KX Lib	14:57:28.00	-21:24:55.7	5.8	K4V	0.076	1.95	n (L09)	n (Be06)
141004	lam Ser	15:46:26.61	+07:21:11.0	12.1	G0IV-V	0.121	2.40	n (A13)	n (K10)
142373	LHS 3127	15:52:40.54	+42:27:05.5	15.9	F8Ve	0.111	2.03	n (A13)	n (T08)
142860	gam Ser	15:56:27.18	+15:39:41.8	11.2	F6IV	0.151	2.93	n (A13)	n (T08)
149661	V2133 Oph	16:36:21.45	-02:19:28.5	9.8	K2V	0.068	1.00	n (E14)	n (T08)
156026	V2215 Oph	17:16:13.36	-26:32:46.1	6.0	K5V	0.064	1.64		n (Be06)
157214	w Her	17:20:39.30	+32:28:21.2	14.3	G0V	0.079	1.01		n (T08)
160915	58 Oph	17:43:25.79	-21:40:59.5	17.6	F5V	0.096	1.18	n (E14)	n (E14)
173667	110 Her	18:45:39.72	+20:32:46.7	19.2	F6V	0.131	2.18	y (A13)	n (T08)
185144	sig Dra	19:32:21.59	+69:39:40.2	5.8	G9V	0.113	2.72	n (A13)	n (T08)
192310	GJ 785	20:15:17.39	-27:01:58.7	8.9	K2+V	0.071	1.25		n (Be06)
197692	psi Cap	20:46:05.73	-25:16:15.2	14.7	F5V	0.136	2.08	n (E14)	n (L09)
201091	61 Cyg A	21:06:53.95	+38:44:58.0	3.5	K5V	0.106	4.43	n (A13)	n (G04)
201092	61 Cyg B	21:06:55.26	+38:44:31.4	3.5	K7V	0.085	3.28	n (A13)	n (G04)
215648	ksi Peg A	22:46:41.58	+12:10:22.4	16.3	F7V	0.132	2.22	n (E14)	n (G13)
219134		23:13:16.98	+57:10:06.1	6.5	K3V	0.080	1.86		n (T08)
222368	iot Psc	23:39:57.04	+05:37:34.6	13.7	F7V	0.137	2.40	n (MG11)	n (B06)

Note. — Excess References: A13=Absil et al. (2013); Be06=Beichman et al. (2006);B06=Bryden et al. (2006); B09=Bryden et al. (2009); E13=Eiroa et al. (2013); E14=Ertel et al. (2014); G13=Gáspár et al. (2013); G03=Greaves & Wyatt (2003); G04=Greaves et al. (2004); K13=Kennedy & Wyatt (2013); K10=Koerner et al. (2010);L02=Laureijs et al. (2002); L09=Lawler et al. (2009); MG11=Millan-Gabet et al. (2011);T08=Trilling et al. (2008)

Eiroa, C., Marshall, J. P., Mora, A., et al. 2013, *A&A*, 555, 11
Ertel, S., Absil, O., Defrère, D., et al. 2014, *A&A*, 570, A128
Fajardo-Acosta, S. B., Telesco, C. M., & Knacke, R. F. 1998, *AJ*, 115, 2101
Fischer, D. A., Marcy, G. W., & Spronck, J. F. P. 2014, *ApJS*, 210, 5
Gáspár, A., Rieke, G. H., & Balog, Z. 2013, *ApJ*, 768, 25
Gillett, F. C. 1986, in *Astrophysics and Space Science Library*, Vol. 124, *Light on Dark Matter*, ed. F. P. Israel, 61–69
Greaves, J. S., Holland, W. S., Jayawardhana, R., Wyatt, M. C., & Dent, W. R. F. 2004, *MNRAS*, 348, 1097
Greaves, J. S., & Wyatt, M. C. 2003, *MNRAS*, 345, 1212
Greene, T., Noecker, C., & ExoPAG SAG 5 team. 2013, *ArXiv e-prints*
Harris, R. J., Andrews, S. M., Wilner, D. J., & Kraus, A. L. 2012, *ApJ*, 751, 115

Hinz, P., Arbo, P., Bailey, V., et al. 2012, in *Society of Photo-Optical Instrumentation Engineers (SPIE) Conference Series*, Vol. 8445, *Society of Photo-Optical Instrumentation Engineers (SPIE) Conference Series*, 0
Hinz, P. M., Solheid, E., Durney, O., & Hoffmann, W. F. 2008, in *Society of Photo-Optical Instrumentation Engineers (SPIE) Conference Series*, Vol. 7013, *Society of Photo-Optical Instrumentation Engineers (SPIE) Conference Series*, 39
Jensen, E. L. N., Mathieu, R. D., & Fuller, G. A. 1996, *ApJ*, 458, 312
Kennedy, G. M., & Wyatt, M. C. 2013, *MNRAS*, 433, 2334
Kennedy, G. M., Wyatt, M. C., Bryden, G., et al. 2014, *TBD*, in press
Koerner, D. W., Kim, S., Trilling, D. E., et al. 2010, *ApJ*, 710, L26

Table 2
Stars in the Sensitivity-Driven Sample

HD	Name	RA	Dec	Distance (pc)	Spectral Type	EEID	F_ν (N-band) (Jy)	hot/warm excess	cold excess
HD 33111	bet Eri	05:07:51.0	-05:05:11.2	27.4	A3IV	0.248	3.72	n (E14)	y (G13)
HD 38678	zet Lep	05:46:57.3	-14:49:19.0	21.6	A2IV-V	0.176	2.06	y (FA98), n (A13)	y (FA98)
HD 40136	eta Lep	05:56:24.3	-14:10:03.7	14.9	F2V	0.161	2.36		y (L09)
HD 81937	h UMa	09 31 31.7	+63:03:42.8	23.8	F0IV	0.168	2.55		n (B06)
HD 95418	beta UMa	11:01:50.5	+56:22:56.7	24.4	A1IV	0.316	4.20	y (FA98), n (A13)	y (S06)
HD 97603	del Leo	11:14:06.5	+20:31:25.4	17.9	A5IV	0.278	3.90	n (A13)	n (G13)
HD 102647	bet Leo	11:49:03.6	+14:34:19.4	11.0	A3V	0.336	6.85	y (A13)	y (S06)
HD 103287	gam Uma	11:53:49.8	+53:41:41.1	25.5	A1IV	0.308	3.69		n (S06)
HD 105452	alf Crv	12:08:24.8	-24:43:44.0	14.9	F1V	0.139	1.97		n (G13)
HD 106591	del UMa	12:15:25.6	+57:01:57.4	24.7	A2V	0.199	2.00	n (A13)	n (G13)
HD 108767	del Crv	12:29:51.8	-16:30:55.6	26.6	A0IV	0.251	2.25	y (E14)	n (S06)
HD 109085	eta Crv	12:32:04.2	-16:11:45.6	18.3	F2V	0.125	1.76	n (A13)	y (W05)
HD 128167	sig Boo	14:34:40.8	+29:44:42.4	15.8	F2V	0.117	1.39		y (L02)
HD 129502	107 Vir	14:43:03.6	-05:39:29.5	18.3	F2V	0.151	2.60	n (E14)	n (G13)
HD 164259	zet Ser	18:00:29.0	-03:41:25.0	23.6	F2IV	0.106	1.14	n (E14)	n (L09)
HD 172167	Vega	18:36:56.3	+38:47:01.3	7.7	A0V	0.916	38.55	y (A13)	y (G86)
HD 187642	Altair	19:50:47.0	+08:52:06.0	5.1	A7V	0.570	21.63	y (A13)	n (R05)
HD 203280	Alderamin	21:18:34.8	+62:35:08.1	15.0	A8V	0.294	7.04	y (A13)	n (C05)
HD 210418	tet Peg	22:10:12.0	+06:11:52.3	28.3	A1V	0.179	1.61	n (E14)	n (S06)
HD 216956	Fomalhaut	22:57:39.0	-29:37:20.0	7.7	A4V	0.504	15.41	y (L13)	y (G86)

Note. — Excess References: A13=[Absil et al. \(2013\)](#); B06=[Bryden et al. \(2006\)](#); C05=[Chen et al. \(2005\)](#); E14=[Ertel et al. \(2014\)](#); FA98=[Fajardo-Acosta et al. \(1998\)](#); G13=[Gáspár et al. \(2013\)](#); G86=[Gillett \(1986\)](#); L02=[Laureijs et al. \(2002\)](#); L09=[Lawler et al. \(2009\)](#); L13=[Lebreton et al. \(2013\)](#); R05=[Rieke et al. \(2005\)](#); S06=[Su et al. \(2006\)](#); W05=[Wyatt et al. \(2005\)](#)

- Kopparapu, R. K., Ramirez, R., Kasting, J. F., et al. 2013, *ApJ*, 765, 131
- Lagrange, A.-M., Desort, M., Galland, F., Udry, S., & Mayor, M. 2009, *A&A*, 495, 335
- Laureijs, R. J., Jourdain de Muizon, M., Leech, K., et al. 2002, *A&A*, 387, 285
- Lawler, S. M., Beichman, C. A., Bryden, G., et al. 2009, *ApJ*, 705, 89
- Lebreton, J., van Lieshout, R., Augereau, J.-C., et al. 2013, *A&A*, 555, A146
- Leconte, J., Forget, F., Charnay, B., Wordsworth, R., & Pottier, A. 2013, *Nature*, 504, 268
- Mason, B. D., Wycoff, G. L., Hartkopf, W. I., Douglass, G. G., & Worley, C. E. 2013, *VizieR Online Data Catalog*, 1, 2026
- Mennesson, B., Millan-Gabet, R., Serabyn, E., et al. 2014, *ApJ*, 797, 119
- Millan-Gabet, R., Serabyn, E., Mennesson, B., et al. 2011, *ApJ*, 734, 67
- Nidever, D. L., Marcy, G. W., Butler, R. P., Fischer, D. A., & Vogt, S. S. 2002, *ApJS*, 141, 503
- Osterloh, M., & Beckwith, S. V. W. 1995, *ApJ*, 439, 288
- Phillips, N. M., Greaves, J. S., Dent, W. R. F., et al. 2010, *MNRAS*, 403, 1089
- Pourbaix, D., Tokovinin, A. A., Batten, A. H., et al. 2009, *VizieR Online Data Catalog*, 1, 2020
- Rieke, G. H., Su, K. Y. L., Stansberry, J. A., et al. 2005, *ApJ*, 620, 1010
- Roberge, A., Chen, C. H., Millan-Gabet, R., et al. 2012, *PASP*, 124, 799
- Spergel, D., Gehrels, N., Breckinridge, J., et al. 2013, *ArXiv e-prints*
- Stark, C. C., Roberge, A., Mandell, A., & Robinson, T. D. 2014, *ApJ*, 795, 122
- Su, K. Y. L., Rieke, G. H., Stansberry, J. A., et al. 2006, *ApJ*, 653, 675
- Trilling, D. E., Bryden, G., Beichman, C. A., et al. 2008, *ApJ*, 674, 1086
- Turnbull, M. C., Glassman, T., Roberge, A., et al. 2012, *PASP*, 124, 418
- Wyatt, M. C., Greaves, J. S., Dent, W. R. F., & Coulson, I. M. 2005, *ApJ*, 620, 492
- Wyatt, M. C., Smith, R., Greaves, J. S., et al. 2007, *ApJ*, 658, 569

Table 3
Binary Stars Excluded from the Sample

HD	Name	SpTyp	Binarity Notes
HD 432	bet Cas	F2IV	WDS says SB with P=27d
HD 4614	eta Cas	G3V	VB 12", 70AU, P=480yr
HD 6582	mu Cas	G5V	VB 1", 7.5 AU + SB
HD 8538	del Cas	A5III-IV	SB, perhaps eclipsing
HD 11443	alf Tri	F6IV	SB, P=1.8d
HD 11636	bet Ari	A5V	SB9, P=107d
HD 13161		A5IV	SB, P=31d, resolved by MarkIII
HD 13974		G0V	SB, P=10d
HD 16970		A2V	VB, 2.3"
HD 20010		F6V	VB 4.4", 62 AU
HD 20630	kap01 Cet	G5V	WDS says SB, but not variable in Nidever et al. (2002)
HD 39587	chil Ori	G0V	VB 0.7", 6 AU, P=14yr
HD 40183		A1IV-V	SB, P=3.7d, resolved by MarkIII
HD 47105		A1.5IV	SB/speckle VB
HD 48915	Sirius	A0V	VB, 7.5"
HD 56986	del Gem	F2V	SB, P=6.1 yr
HD 60179	Castor A	A1.5IV	SB, P=9.2d plus VB, P=467 yr
HD 61421	Procyon	F5IV	VB 5", 18AU, P=40 yr and SB
HD 76644		A7V	SB, P=11yr
HD 76943	10 UMa	F3V	SB/VB 0.6", P=21.8 yr
HD 82328	tet UMa	F7V	WDS says SB (SBC7), but not in SB9, also VB, 5"
HD 82885	SV Lmi	G8III	VB 3.8", 43 AU, P=200 yr
HD 95735		M2V	EB
HD 98231	GJ 423A	G0V	Complicated multiple system
HD 104304		G8IV	VB, 1"
HD 109358	bet Cvn	G0V	SB, 0.1", 1.3 AU
HD 110379	GJ 482A	F0V	VB, 3.75", 44AU, P=171yr
HD 112413	alf02 CVn	A0II-III	SB
HD 114378J	alph Com	F5V	VB 0.7", 12 AU, P=26yr
HD 114710	bet Com	G0V	possible SB
HD 116656	Mizar A	A1.5V	SB, P=20.5d
HD 118098	zet Vir	A3V	VB, companion is M4-M7
HD 121370	eta Boo	G8V	SB9, P=494d
HD 130841	alf Lib A	A4IV-V	possible SB
HD 131156	37 Boo	G8V	VB 4.9", 33AU, P=151yr
HD 131511	GJ 567	K2V	possible SB P=125d
HD 133640	GJ 575	G0V	VB, 3.8", 48 AU (now at 1.5")
HD 139006	alf CrB	A1IV	SB, P=17d
HD 140538		G2.5V	VB, 4.4", 65 AU
HD 144284	tet Dra	F8 IV-V	SB, P=3.1d
HD 155125		A2IV-V	VB 0.86"
HD 155886	GJ 663A	K2V	VB 5", 28 AU
HD 155885	36 Oph	K2V	VB 15", 87AU, P=569yr + possible SB
HD 156164	del Her	A1IV	SB 0.1"
HD 156897	40 Oph	F2V	VB, approx 4" (CCDM)
HD 159561	alf Oph	A5II	VB 0.8"
HD 160269		G0V	VB 1.5", 21 AU
HD 160346	GJ 688	K3V	SB P=84d
HD 161797	mu Her	G5IV	VB 1.4", 12AU, P=65yr
HD 165341	70 Oph A	K0V	VB 4.6", 23AU, P=88yr
HD 165908	b Her	F7V	VB 1.1", 17 AU, P=26 yr
HD 170153		F7V	SB 0.1", 1AU, P=0.8yr
CCDM 19026-2953 A		A2.5V	VB 0.53"
HD 177724		A0IV-V	SB + VB, 5"
HD 182640	del Aql	F1IV-V	SB, resolved at 0.1"
HD 185395	tet Cyg	F4V	VB/SB, approx 2.5"
HD 207098	del Cap	F2III	EB
HD 210027	iot Peg	F5V	SB1, P=10d
HD 224930	85 Peg	G5V	VB 0.8", 10AU, P=26 yr